Original article

Uncollimated scintigram image restoration

Naoki Kubo, Hiroyuki Hanada

Abstract

We have conducted an experiment on restoring scintigram images obtained without the use of collimators. Uncollimated images of liver slice phantoms filled with ^{99m}Tc were taken at a phantom-camera distance of 0 cm. The sensitivity under these conditions was about one thousand times higher than that using a low-energy high-resolution collimator. Uncollimated images were restored using unsharp masking in combination with spatial filtering. The unsharp masking process involved subtracting two images taken at phantom-camera distances of 0 and 2.3 cm to produce a difference image. The mean squared errors found were 0.56 for the uncollimated images, 0.54 for the images processed with the spatial filter only, and 0.53 for the images produced using unsharp masking followed by spatial filtering. Thus, the images processed using both unsharp masking and the spatial filter bore the closest resemblance to the actual images. Also, since this method was capable of revealing the shape of the phantom, it may already be usable for imaging large lesions, such as in lung perfusion scintigraphy.

1. Introduction

Scintigrams are images produced by γ-rays emitted by radiopharmaceuticals internally administered to patients. The distribution of radiopharmaceuticals can be digitized and analyzed. This has enabled physicians to readily identify abnormal biogenic activities occurring in internal organs.

Currently, the Anger scintillation camera (hereinafter "camera") is the device commonly used for scintigraphy. The camera always has an attached collimator. As can be seen in Fig. 1, the collimator passes the γ-rays emitted from the subject only in one fixed direction, so it plays a role in producing the γ-ray image at the detector. It corresponds to the lens in an optical camera. Physically, it takes the form of a large array of lead apertures.

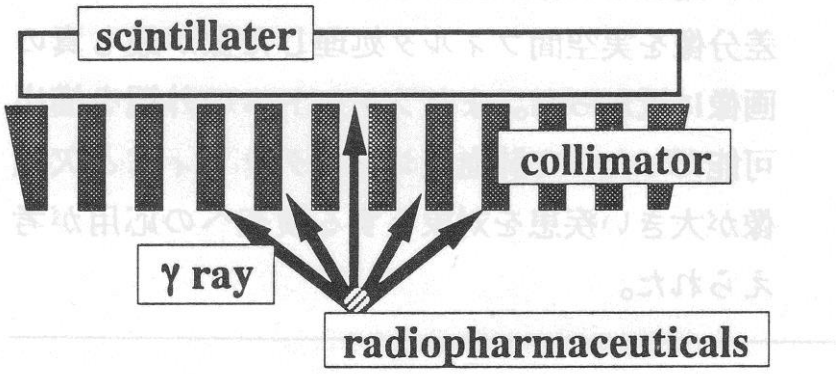

Figure 1 Schematic diagram of collimator

Since the collimator blocks most of the γ-rays emitted from the subject, this drastically reduces the sensitivity of the instrument. This is why the sensitivity of the camera is determined by the counting efficiency of the scintillator and the efficiency of the collimator.

It follows that if we use a scintillator detector without a collimator, we can expect dramatic improvements in sensitivity. However, no clear image will be formed in such a situation (uncollimated image). If it was possible to extract meaningful diagnostic information from such a scintigram, though, this would greatly shorten the examination time and allow the physician to reduce the amount of radiopharmaceutical administered. In the present study, image-processing was employed on uncollimated scintigrams in an attempt to restore the image.

2. Theory

2.1 Image restoration methods, Part 1: The restoration filter

Images that have become degraded by spatial blurring can be recovered with a restoration filter. This filter is capable of simultaneously correcting spatial blur and suppressing statistical noise, and plays an important role in nuclear medicine image processing. In this usage, sometimes its 1-dimensional spatial frequency characteristics are tuned to employ it as a spatial filter.

The following expression is used as a restoration filter:

$$W(f) = \frac{e^{-\pi^2 \cdot f^2 \cdot m^2 / 2.773}}{(e^{-\pi^2 \cdot f^2 \cdot m^2 / 2.773})^2 + c} \quad , \qquad (1)$$

where *f* is the 1-dimensional spatial frequency and *m* and *c* are parameters determining the filter characteristics.

2.2 Image restoration methods, Part 2: Unsharp masking

One means for recovering a degraded image due to spatial blurring is unsharp masking. In this 3-step process, first, the original image f(x,y) is processed to create the unsharp mask h(x,y); this means that only the low spatial frequency components are extracted from the original image. Next, that image is subtracted from the original image to obtain the difference image. Finally, this difference image is multiplied by some coefficient and added to the original image. This is formulated as follows:

$$g(x,y) = f(x,y) + K \cdot \{ f(x,y) - f(x,y) * h(x,y) \} \quad , \qquad (2)$$

where *g(x,y)* is the restored image, *K* is the weighting factor, and * represents the convolution. The nature of unsharp masking means that it only restores spatial blurring.

2.3 Application of unsharp masking

The authors have developed a theoretically-based procedure for unsharp masking. This method starts by collecting images under two different observation conditions. The first simply corresponds to the condition of the original observation, and the second incorporates spatial blurring, i.e., the unsharp masking condition. If the weighting factor K in Eq. (2) is made relatively large, the first term can be neglected and the equation can be approximated by the second term. In the proposed unsharp masking process, the observed image is then subtracted from the original image to obtain the difference image. The key characteristic of this procedure is that the step involving application of the mask *h(x,y)* is omitted. In this way, arbitrariness can be eliminated from the magnitude of the convolution kernel of *h(x,y)* (the masking calculation domain). In the final step, the restoration filter is employed to suppress noise.

3. Method

3.1 Equipment and specimens

The scintillation camera was a GCA-602A (Toshiba Co.). The phantoms were International Atomic Energy Agency liver slice phantoms (Kyoto Kagaku Co., Ltd.). They measured 20 cm high by 13 cm wide and incorporated 8 circular voids, the largest of which was 4 cm in diameter.

3.2 Measurement of sensitivity

The following measurements were performed in order to compare the sensitivities of a scintillator with and without a low-energy, high-resolution collimator attached. The subjects of the imaging were liver slice phantoms (hereinafter, phantoms) injected with 4.2 MBq of ^{99m}Tc solution. The stock software in the camera system was used to take the measurements. The unit was counts/second (cps).

3.3 Collection of uncollimated phantom images

The phantoms described in Sect. 3.2 were imaged in a 128 × 128 matrix and the count was 5000 kcounts. The source-camera distance (hereinafter, distance) was 0 cm.

3.4 Processing using restoration filter only

The uncollimated images taken using the method described in Sect. 3.3 were processed with a restoration filter based on Eq. (1). Since no optimal values are known for the parameters, *m* was set at 1.0, 3.0, 5.0, 7.0 and 9.0. The following values for *c* were used in combination with each *m* value: 1.0×10^{-3}, 2.0×10^{-3}, 3.0×10^{-3}, 4.0×10^{-3}, 5.1×10^{-2}, 1.0×10^{-1} and 1.5×10^{-1}. Thus, a total of 35 parameter combinations were employed during processing with the filter. Each image was transformed using a spatial filter with dimensions of 25 × 25 pixels.

3.5 Evaluation of point spread function

The point spread function was evaluated before carrying out the unsharp masking procedure. The point source consisted of a 400 kBq ^{99m}Tc solution. Data was collected in a 128 × 128 matrix at a count of 5000 kcounts. No collimator was attached.

Two distances were used, 0 cm and 2.3 cm, with a Styrofoam sheet between the camera and the source. The profile curve of the gathered point images was measured and the point spread function and full width at half maximum (FWHM) were calculated.

3.6 Application of unsharp masking

The conditions described in Sect. 3.5 were found to produce more blurred images at a distance of 2.3 cm than at 0 cm, so phantom images were collected at 2.3 cm. Other than the distance, the conditions were those described in Sect. 3.3. Difference images were created by subtracting these images from the previously taken image at 0 cm. The 35 filters described in Sect. 3.4 were then used to process each difference image.

3.7 Evaluation of images

The mean squared error is an index of how reliably the obtained images match the actual image. This is determined using the following expression:

$$NMSE = \frac{\sum_{l=1}^{L}\sum_{m=1}^{M}(r'_{lm} - b_{lm})^2}{\sum_{l=1}^{L}\sum_{m=1}^{M} b_{lm}^{\ 2}} \quad ,$$

where $\underline{b_{lm}}$ indicates the actual image of the phantom.
r'_{lm} represents the images gathered using the three methods, *without* the collimator as in Sect. 3.3, *with only* the restoration filter as in Sect. 3.4, and with unsharp masking as in Sect. 3.6. A 1 × 2 cm region of interest was selected from the center of this image and the mean was normalized to 50 counts to match each of the images.

3.8 Level of spatial blurring

The Nitka method was modified to find the level of spatial blurring, i.e., the region of interest was defined as a shape matching the outline of the phantom in the normalized image from Sect. 3.7. A total count was taken from everywhere outside that region. The lower the count, the less the spatial blurring; this meant that there was no spreading of the image into locations beyond the boundaries of the phantom.

4. Results

4.1 Sensitivity

The sensitivity was 1.78×10^{-1} kcps when a low-energy, high-resolution collimator was attached. Without a collimator, on the other hand, the sensitivity was a thousand times as high, at 1.80×10^{2} kcps.

4.2 Uncollimated phantom images

Figure 2 shows an uncollimated image, and the solid line indicates the actual outline of the phantom. It can be seen that the image has spread beyond this outline. Also, the 4-cm void is not very clearly reproduced.

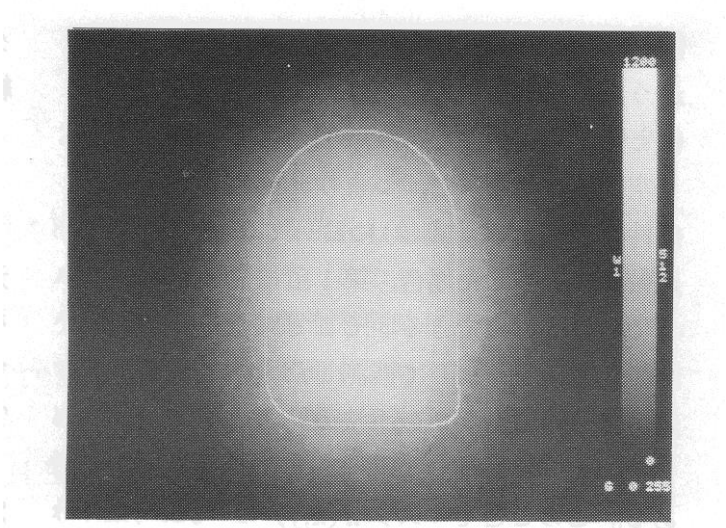

Figure 2 Uncollimated image at phantom-camera distance of 0 cm. White line indicates outline of actual phantom.

4.3 Source-camera distance and point spread function

Figure 3 shows the point spread functions measured in this study. At the distance of 0 cm, the FWHM was 74.5 mm, and at 2.3 cm, it was 113.0 mm. This figure confirms that the image taken from a distance of 2.3 cm was more blurred; therefore, the method described in Sect. 3.6 was used.

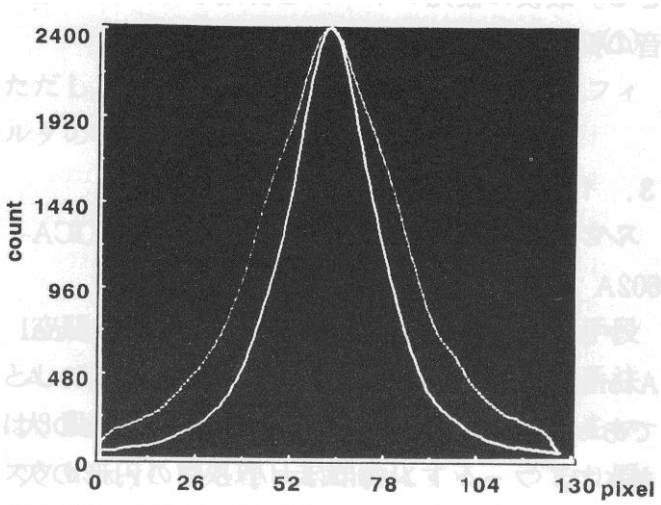

Figure 3 Point spread functions. Solid and dotted lines represent source-camera distances of 0 and 2.3 cm, respectively.

4.4 Restored images and assessment

The mean squared error of the uncollimated images before restoration was 0.56.

The mean squared error for the best image among all those obtained by processing with the 35 filters was 0.54 for the uncollimated images using the restoration method described in Sect. 3.4, and 0.53 for the images obtained using the restoration method based on unsharp masking images described in Sect. 3.6.

Figure 4 shows the best version of the restored uncollimated image. The spatial frequency characteristics of the filter used to obtain this image are shown in Fig. 5. Figure 6 shows the restoration achieved by the best filter using the unsharp masking image described in Sect. 3.6, and Fig. 7 shows the spatial frequency characteristics of that filter.

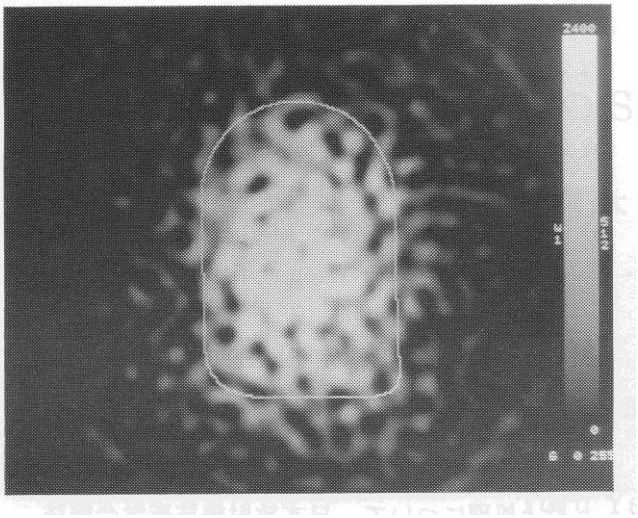

Figure 4 Restoration of uncollimated image taken at phantom-camera distance of 0 cm. White line indicates outline of actual phantom.

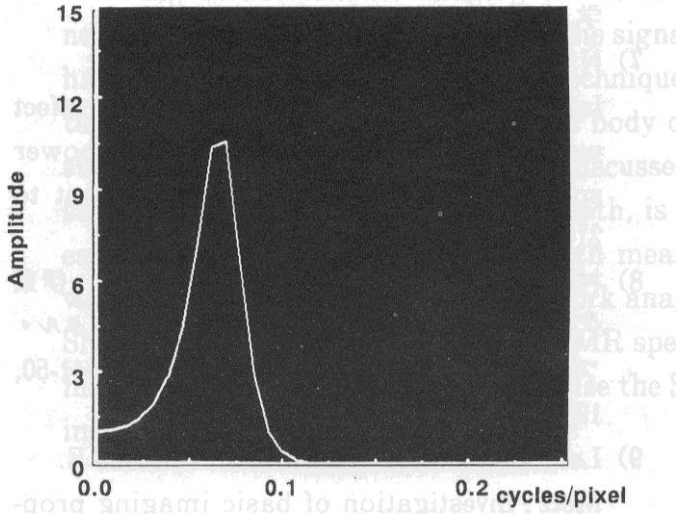

Figure 5 Spatial frequency characteristics of filter used for restoration shown in Figure 4. Parameter m was 7.0 and parameter c was 2.0×10^{-3}.

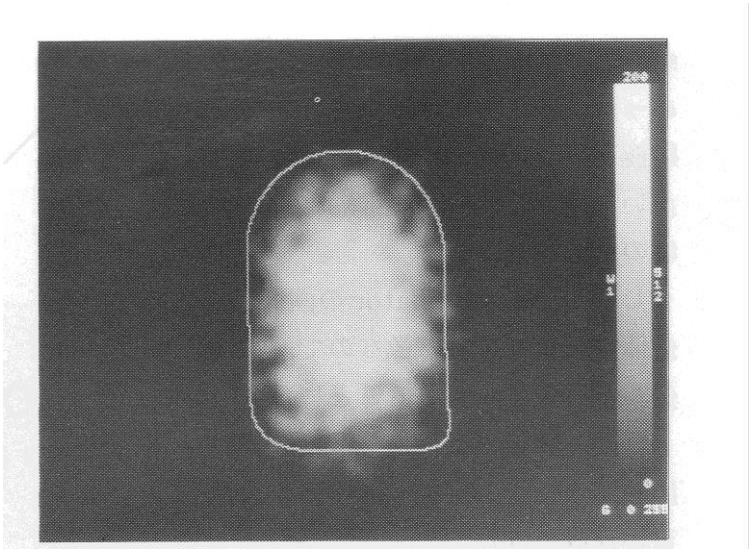

Figure 6 Restoration achieved using the unsharp masking image. White line indicates outline of actual phantom.

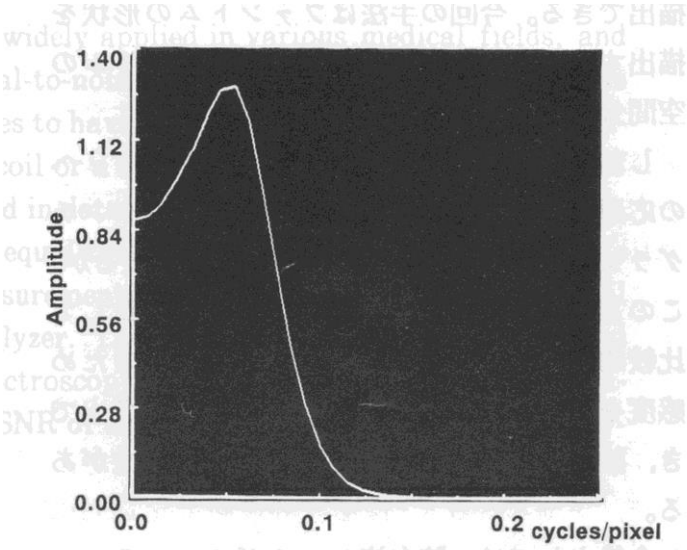

Figure 7 Spatial frequency characteristics of filter used for restoration shown in Figure 6. Parameter m was 5.0 and parameter c was 1.5×10^{-1}.

The mean squared error results indicate that restoration based on the unsharp masking image produces an image most closely resembling the actual one. Nevertheless, the 4 cm void is not very well reproduced in Fig. 6.

4.5 Level of spatial blurring

The count in the region outside the region of interest, defined by the outline of the phantom, was 99,547 in the uncollimated image and 50,384 in the restored image. In contrast, it was 26,345 in the image restored using the unsharp masking image; this represents a sizeable reduction compared to the other images. This indicates that among these methods, restoration using the unsharp masking image produces the lowest amount of spatial blurring, in other

words, the minimal image spread.

5. Observations

The sensitivity for the uncollimated images was one thousand times higher than that using the low-energy, high-resolution collimator. This means less burden on the patient; the radiation from the radiopharmaceuticals ingested by the patient can be greatly reduced, or alternatively, the examination time can be greatly shortened.

Since the raw uncollimated images are extremely blurred, however, they do not really constitute “images” of the distribution of the radiopharmaceutical.

In the present study, an application of unsharp masking is used in order to create images of phantoms.

Let us turn to the clinical applicability of this procedure. Currently, scintigrams are capable of imaging distributions with sizes of several millimeters. The present procedure is only capable of approximating the shape of a phantom, and it does not provide the spatial resolution of a scintigram.

Nonetheless, this procedure appears to be applicable to lung perfusion scintigraphy, which can be used to detect lung embolism. In this case, the defective regions are relatively large, coinciding with a subsegment or a lobe. Thus, the proposed procedure may provide useful imaging in such a situation.

In a future study, a phantom will be created for lung perfusion scintigraphy, the diagnostic reliability of the proposed method will be investigated, and further research conducted into better image restoration methods.

6. Summary

A procedure was developed that uses both unsharp masking and a restoration filter. This procedure was demonstrated to be capable of restoring uncollimated scintigrams.

References

Madsen MT: A method for obtaining an approximate Wiener filter. *Med. Phys.* 17(1):126-130, 1990

Kubo N, Kanegae K, Katoh C, et al.: Improvement of the partial volume effect using a filter based on a projection power spectrum. *Eur. J. Nucl. Med.* 21(10), s133, 1994

Loo LN, Doi K, Metz CE: Investigation of basic imaging properties in digital radiography. 4. Effect of unsharp masking on the detectability of simple patterns. *Med. Phys.* 12(2):209-214, 1985

Penney BC, King MA, Schwinger RB, Baker SP, Stritzke P, Doherty PW: Constrained least-squares restoration of nuclear medicine images: selecting the coarseness function. *Med. Phys.* 14(5):849-858, 1987